Preprint Title Density of states in the presence of spin dependent scattering: numerical and analytical approach

Authors Tairzhan Karabassov, Valeriia D. Pashkovskaia, Nikita A. Parkhomenko, Anastasia V. Guravova, Elena A. Kazakova, Alexander A. Golubov and Andrey S. Vasenko

Publication Date 29 Jun 2022

Article Type Full Research Paper

ORCID® iDs Tairzhan Karabassov - https://orcid.org/0000-0001-7966-5221

Density of states in the presence of spin dependent scattering: numerical and analytical approach

T. Karabassov[1], V. D. Pashkovskaia[1], N. A. Parkhomenko[1], A. V. Guravova[1], E. A. Kazakova[2], A. A. Golubov[3] and A. S. Vasenko*[1,4]

Address: [1]HSE University, 101000 Moscow, Russia; [2]Sechenov First Moscow State Medical University, 119991 Moscow, Russia; [3]Faculty of Science and Technology and MESA+ Institute for Nanotechnology, University of Twente, 7500 AE Enschede, The Netherlands and [4]I.E. Tamm Department of Theoretical Physics, P.N. Lebedev Physical Institute, Russian Academy of Sciences, 119991 Moscow, Russia

Email: A. S. Vasenko - avasenko@hse.ru

* Corresponding author

Abstract

We present the quantitative study of the density of states (DOS) in SF bilayers (where S - is a bulk superconductor and F - a ferromagnetic metal) in the diffusive limit. We solve the quasiclassical Usadel equations in the structure, considering the presence of magnetic and spin-orbit scattering. For practical reasons we propose the analytical solution for the density of states in SF bilayer in case of thin ferromagnet and low transparency of the SF interface. It is confirmed by numerical calculations, using a self-consistent two-step iterative method. The behavior of DOS dependencies on magnetic and spin-orbit scattering times is discussed.

Keywords

Density of states, Josephson junctions, proximity effect, superconductivity, Superconductor/Ferromagnet hybrid nanostructures

Introduction

It is well-known that superconductivity can be induced into a non-superconducting metal in the hybrid structures due to the proximity effect [1-7]. For instance, in NS bilayers (where N denotes a normal metal and S - a superconductor) the superconducting correlations penetrate into the normal metal layer over a characteristic decay length ξ_n. When a superconductor S is combined with a ferromagnetic layer F forming SF bilayer, the superconductivity leaks into the ferromagnetic region over $\xi_h \propto 1/\sqrt{h}$, where h is the exchange field in the ferromagnetic layer [1]. Not only superconductivity is substantially suppressed due to the exchange field, but also Cooper pairs gain a finite center of mass momentum which leads to the oscillatory behavior of the Cooper pair wavefunction. These oscillations can be described in the diffusive limit in the framework of the so called Usadel equations which are written in terms of the quasiclassical Green's functions. Such approach proved to be very powerful for the description of the proximity effect in the diffusive superconducting hybrids [1-3,8-10].

The scientific community has been examining the proximity effect in SF hybrid structures already for a long while. It has been found that the oscillatory behavior of the superconducting wavefunction can lead to various interesting phenomena which can be observed experimentally[1,2]. For instance, the superconducting transition temperature shows non-monotonous and in some cases oscillatory behavior in the multilayered SF structures [11-15]. Recently, it has been shown theoretically that similar behavior can be observed in S/TI structures with non-uniform magnetization pattern on the surface of a 3D topological insulator (TI) [16]. The Josephson critical current demonstrates the damped oscillatory behavior as a function of thickness of the ferromagnetic layer in SFS Josephson junctions [17-45]. Similarly, the density of states (DOS) also demonstrates the damped oscillatory dependence as a function of F layer thickness in SF systems [46-50].

The density of states is one of the crucial spectral characteristics of the proximity effect in superconducting hybrid structures. For example, the DOS calculation is essential for the quasiparticle current computation in SIFS (where I denotes an insulatung layer) [27,49,51-55] or SFIFS tunneling Josephson junctions [56]. Therefore computation of DOS is also needed for many actively studied areas of research, including the thermospin [57,58] and thermoelectric [59-64] effects, spin and heat valves [65-73] as well as nanosize refrigerators [63,74-76], etc. Presently the DOS structure at the free edge of a normal metal layer in NS bilayers is well-known [1-3,77]. It has the so-called mini-gap at the subgap energies $E < \Delta$ (where Δ is the superconducting gap), whose magnitude depends on the NS interface parameters and N layer thickness [77,78]. Replacing the N layer with a ferromagnetic metal F results in a more sophisticated DOS structure, since there is a non-zero exchange field, which causes the spin-split densities of states for two spin populations of electrons [1-3,79]. More general consideration should also include possible spin-flip as well as spin-orbit scattering processes in the ferromagnetic region [80].

In this work we consider the SF bilayer, assuming relatively low interface transparency and the presence of magnetic and spin-orbit scattering. For that purpose the Kupriyanov-Lukichev (KL) boundary conditions at the superconductor/ ferromagnet interface are perfectly suitable [81]. Previously, the DOS in SF bilayers has been studied numerically [82,83]. We revisit this question and propose an analytical model to describe the influence of spin-flip and spin-orbit scattering on the DOS behavior. Then we provide a comparison with the exact numerical calculation using a self-consistent two-step iterative method. Furthermore, we briefly discuss the consequences of the different scatterings on the current-voltage characteristics in SFIFS junctions. We do not consider any additional effects in the SF boundary such as spin-dependent interfacial phase shifts (SDIPS). The effect of SDIPS on DOS behavior in SFIFS junctions has been studied both analytically [84] and numerically [85].

The paper is organized as follows. In the section ("Model") we formulate the theoretical model. In the following sections the derivation of analytical results is presented. We discuss the calculations in the section ("Results") and finally we summarize the results in the last section ("Conclusion").

Model

The theoretical model of the SF structure under consideration is depicted in Fig. . It consists of a ferromagnetic layer with thickness d_f and a superconducting electrode along the x direction. S/F interface is characterized by the dimensionless parameter $\gamma_B = R_B \sigma_n / \xi_f$, where R_B is the resistance of the S/F interface, σ_n is the conductance of the F layer [86,87], $\xi_f = \sqrt{D_f / 2\pi T_c}$, D_f is the diffusion coefficient in the ferromagnetic metal, and T_c is the critical temperature of the superconductor [1,2]. We assume $\hbar = k_B = 1$. We also assume that the S/F interface is not magnetically active. We will consider the diffusive limit in this model and neglect the nonequilibrium effects in the structure [88-90].

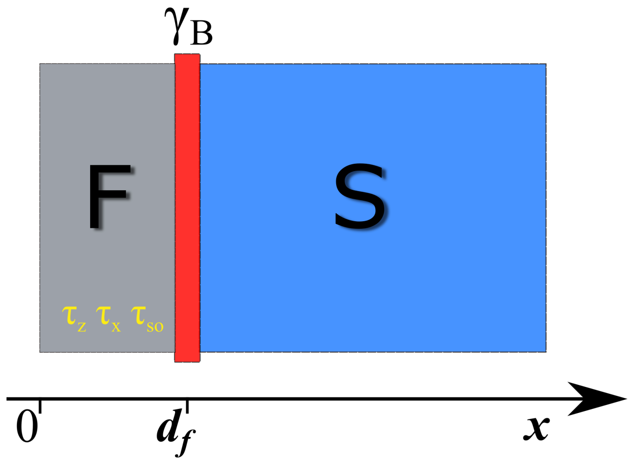

[t]

Figure 1: Geometry of the SF bilayer. We consider the S/F interface to be a tunnel barrier. Here γ_B is the interface transparency parameter.

The goal is to find the DOS of a single SF bilayer, which can be done by solving the Usadel equations in the ferromagnetic and superconducting layers.

Using the θ parametrization of the normal and anomalous quasiclassical Green's functions, $G = \cos\theta$ and $F = \sin\theta$, respectively, we can write the Usadel equations in F layer as [4,49,80,82,91]

$$\frac{D_f}{2} \frac{\partial^2 \theta_{f\uparrow(\downarrow)}}{\partial x^2} = (\omega \pm ih + \frac{1}{\tau_z} \cos\theta_{f\uparrow(\downarrow)}) \sin\theta_{f\uparrow(\downarrow)} \\ + \frac{1}{\tau_x} \sin(\theta_{f\uparrow} + \theta_{f\downarrow}) \pm \frac{1}{\tau_{so}} \sin(\theta_{f\uparrow} - \theta_{f\downarrow}), \quad (1)$$

where the positive and negative signs correspond to the spin-up ($\uparrow$) and spin-down ($\downarrow$) states, respectively. In terms of the electron fermionic operators ψ, the spin-up state corresponds to the anomalous Green's function $F_\uparrow \sim \langle \psi_\uparrow \psi_\downarrow \rangle$, while the spin-down state corresponds to $F_\downarrow \sim \langle \psi_\downarrow \psi_\uparrow \rangle$. We use the Matsubara Green's functions, so $\omega = 2\pi T(n + 1/2)$ are the Matsubara frequencies

[92]. The exchange field of the ferromagnet is h, and the scattering times are labeled here as τ_z, τ_x and τ_{so}. The parameter $\tau_{z(x)}$ corresponds to the magnetic scattering parallel (perpendicular) to the quantization axis, and τ_{so} is the spin-orbit scattering time [80,82,93]. In S layer the Usadel equation has the following form [91],

$$\frac{D_s}{2}\frac{\partial^2\theta_s}{\partial x^2} = \omega\sin\theta_s - \Delta(x)\cos\theta_s. \tag{2}$$

Here D_s is the diffusion coefficient in the superconductor and $\Delta(x)$ is the superconducting order parameter (pair potential). Equations (1) and (2) should be supplemented with the self-consistency equation for the coordinate dependence of superconducting order parameter Δ,

$$\Delta(x)\ln\frac{T_c}{T} = \pi T\sum_{\omega>0}\left(\frac{2\Delta(x)}{\omega} - \sin\theta_{s\uparrow} - \sin\theta_{s\downarrow}\right). \tag{3}$$

The resulting system must be complemented by the boundary conditions at the outer boundary of a ferromagnet,

$$\left(\frac{\partial\theta_f}{\partial x}\right)_{x=0} = 0, \tag{4}$$

and Kupriyanov-Lukichev boundary conditions at the F/S interface [81],

$$\xi_f\gamma\left(\frac{\partial\theta_f}{\partial x}\right)_{x=d_f} = \xi_s\left(\frac{\partial\theta_s}{\partial x}\right)_{x=d_f}, \tag{5}$$

$$\xi_f\gamma_B\left(\frac{\partial\theta_f}{\partial x}\right)_{x=d_f} = \sin(\theta_s-\theta_f)_{x=d_f}. \tag{6}$$

Here $\gamma = \xi_s\sigma_n/\xi_f\sigma_s$, σ_s is the conductivity of the S layer, and $\xi_s = \sqrt{D_s/2\pi T_c}$ is the superconducting coherence length. The parameter γ determines the strength of superconductivity suppression in S layer by the ferromagnet (F layer). We assume that $\gamma \ll 1$, i. e. there is almost no superconductivity suppresion.

To complete the boundary problem, we also set a boundary condition at $x = +\infty$,

$$\theta_s(+\infty) = \arctan\left(\frac{\Delta}{\omega}\right), \tag{7}$$

where the Green's functions take the well-known bulk BCS form. The Green's function technique allows us to compute the DOS at the outer F boundary by solving the resulting system of equations above.

The DOS at the outer F boundary $N_f(E)$ is normalized to the DOS in the normal state and can be written as

$$N_f(E) = [N_{f\uparrow}(E) + N_{f\downarrow}(E)]/2, \tag{8}$$

where $N_{f\uparrow(\downarrow)}(E)$ are the spin-resolved DOS written in terms of spectral angle θ,

$$N_{f\uparrow(\downarrow)}(E) = \mathrm{Re}[\cos\theta_{f\uparrow(\downarrow)}(i\omega \to E + i0)]. \tag{9}$$

To calculate (9), we use a self-consistent two-step iterative method. In the first step we calculate the pair potential coordinate dependence $\Delta(x)$ using the self-consistency equation (3) in S layer. Then, by proceeding to the analytical continuation in (1) and (2) over the quasiparticle energy $i\omega \to E+i0$ and using $\Delta(x)$ dependence obtained in the previous step, we find the Green's functions by repeating the iterations until convergency is reached.

The DOS in the limit of small F-layer thickness

In this section we find the analytical result assuming $d_f \ll min(\xi_f, \sqrt{D_f/2h})$, so it is case of a thin and weak ferromagnet. Under the condition $\gamma_B/\gamma \gg 1$ we can neglect the suppression of superconductivity in the superconductor. We will keep all the scattering terms in the solution to obtain more general result. In this case we can expand the solution of the Usadel equations up to the second order in small spatial gradients. The θ_f functions can be approximated in the following way

$$\theta_{f\uparrow} = A + Bx + Cx^2, \tag{10}$$

$$\theta_{f\downarrow} = A^* + B^*x + C^*x^2. \tag{11}$$

where * is the complex conjugation and the coefficients A, B, C are determined from the boundary conditions.

Inserting the solution (10) into the Usadel equation in the F layer Eq. (1), we get,

$$C = \frac{1}{2}\left[(\omega_n + ih)\sin A + \frac{1}{2}\alpha_z \sin 2A\right] + \\ + \frac{1}{2}\left[\alpha_x \sin(A + A^*) + \alpha_{so}\sin(A - A^*)\right]. \tag{12}$$

For convenience we introduced the scattering rate parameters: $\alpha_z = 1/\tau_z\Delta$, $\alpha_x = 1/\tau_x\Delta$ and $\alpha_{so} = 1/\tau_{so}\Delta$. To find the coefficients we utilize the boundary conditions (4) and (6),

$$(B + 2Cx)_{x=0} = 0, \tag{13}$$

$$\xi_f\gamma_B\,(B + 2Cx)_{x=d_f} = \sin(\theta_s - A)|_{x=d_f}. \tag{14}$$

From the first equation we obtain $B = 0$, while the second equation results in the expression for A. Now we will discuss a ferromagnet with a strong uniaxial anisotropy, in which case the perpendicular fluctuations of the exchange field are suppressed ($\tau_x^{-1} \sim 0$). For simplicity we also assume the ferromagnet with weak spin-orbit interactions and also neglect the spin-orbit scattering time τ_{so}. Finally, assuming $\tau_x^{-1}, \tau_{so}^{-1} = 0$ and keeping the solution to the lowest order, the equation for θ_f takes form,

$$\gamma_B d_f\,(\omega_n \pm ih)\tan\theta_{f\uparrow(\downarrow)} + \\ + \cos\theta_s \tan\theta_{f\uparrow(\downarrow)} + \alpha_z\gamma_B d_f \sin\theta_{f\uparrow(\downarrow)} = \sin\theta_s, \tag{15}$$

where $\sin\theta_s = \Delta_0/\sqrt{\omega_n^2+\Delta_0^2}$ and $\cos\theta_s = \omega_n/\sqrt{\omega_n^2+\Delta_0^2}$. Here Δ_0 is a bulk value of the pair potential. The equation above can be used for further semi-analytical calculations of the DOS for the thin F layer case with the magnetic scattering rate α_z. When $\alpha_z = 0$ the equation (15) reduces to the well-known result (see, for example, Ref. [79] or Ref. [84]),

$$\tan\theta_{f\uparrow(\downarrow)} = \frac{\sin\theta_s}{(\omega_n \pm ih)\,\gamma_B d_f + \cos\theta_s}. \tag{16}$$

Analytical solution in the low proximity limit and small F-layer thickness

In this section we perform further analytical calculation of the anomalous Green's function in the F layer based on the results of the previous section. We then analyze the effect of various scattering rates on the superconducting correlations, including odd-frequency triplet component which is generated in the adjacent ferromagnet.

The expression for θ-parameterized Green's functions can be found from the boundary conditions (13),

$$\begin{aligned}&\gamma_B d_f\left[(\omega_n \pm ih) + \alpha_z\cos\theta_{f\uparrow(\downarrow)}\right]\sin\theta_{f\uparrow(\downarrow)} +\\ &+\gamma_B d_f\left[\alpha_x\sin\left(\theta_{f\uparrow}+\theta_{f\downarrow}\right) \pm \alpha_{so}\sin\left(\theta_{f\uparrow}-\theta_{f\downarrow}\right)\right] =\\ &=\sin\left(\theta_s-\theta_{f\uparrow(\downarrow)}\right).\end{aligned} \tag{17}$$

In order to simplify the calculation and the final form of the solution θ_f we consider only positive Matsubara frequencies ω_n and perform further linearization of the Eq. (17) which is justified in the low proximity limit. Then we obtain,

$$\theta_{f\uparrow(\downarrow)} = \\ = \frac{\sin\theta_s\left(1+\gamma_B d_f\left(\alpha_z+2\alpha_{so}+\omega_n\mp ih\right)\right)}{\gamma_B^2 d_f^2\left[h^2-\left(\alpha_x-\alpha_{so}\right)^2\right]+\left[1+\gamma_B d_f\left(\Sigma\alpha_i+\omega_n\right)\right]^2}. \tag{18}$$

Here, $\Sigma\alpha_i$ denotes the sum of all the scattering rates.

The above solution is true for thin ferromagnetic layers in the low proximity limit. More general analytical solution can be obtained for arbitrary thicknesses in frame of the linearized Usadel equations. In order to find the DOS in the proposed limit we expand the θ-parametrized normal Green's function around small value of θ_f. In this case we have,

$$N_{f\uparrow(\downarrow)}\left(E\right)\approx 1-\frac{1}{2}Re\left[\theta^2_{f\uparrow(\downarrow)}(\omega_n\to -iE)\right], \tag{19}$$

and to calculate the total DOS we need to sum the contributions from two spin populations using Eq. (8).

Results

In the present section we outline the main results, including both numerical and analytical calculations. The following parameters are fixed throughout the section: $T = 0.1T_c$, $\gamma = 0.05$ and $d_f = 0.5\xi_n$. First, we discuss general features of the DOS in an SF bilayer in the absence of any scattering. Then the effect of the spin-dependent scattering on the key DOS features in two relevant cases is discussed (see below) and finally, we present the analytical result and compare it with the numerically calculated DOS.

Evolution of the DOS in SF bilayer

It is instructive to discuss the key features of the DOS in an SF bilayer first. That is why, in this section we briefly discuss the evolution of the DOS for different values of the exchange field h and

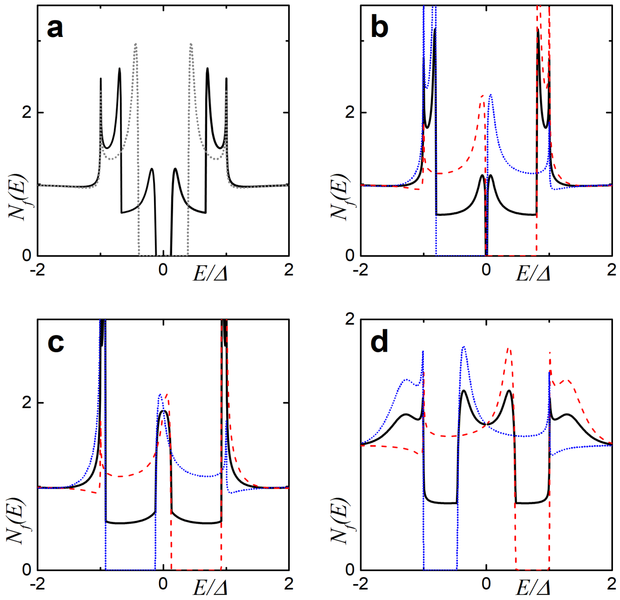

Figure 2: The evolution of the DOS plotted for increasing values of the exchange field h. Here $\gamma_B = 5, d_f = 0.5$. In plot (a) black dotted line represents the $h = 0$ case (i.e. the NS bilayer). In plots (a)-(d) black solid lines correspond to the total DOS, while red dashed lines show $N_{f\uparrow}(E)$ and blue dash-dotted lines show $N_{f\downarrow}(E)$. (a) black solid line calculated for $h = 0.4\Delta$, and all lines are calculated for: (b) $h = 0.8\Delta$, (c) $h = \Delta$ and (d) $h = 1.6\Delta$.

barrier transparencies γ_B. All the scattering is assumed to be absent for simplicity $\alpha_m = \alpha_x = \alpha_{so} = 0$ in this subsection.

In Fig. 2 we observe the influence of an increasing exchange field h on the DOS structure calculated for $\gamma_B = 5$, in particular we can see the evolution of the DOS peaks. For $h = 0$, i.e. the case of SN bilayer we see the well-known DOS structure with the characteristic mini-gap at energies $E < \Delta$ (Fig. 2 (a) black dotted line) [77] . This proximity-induced mini-gap originates from the effective backscattering of the quasiparticles at the S/N interface due to a finite interface resistance [94]. As h increases the DOS splits for the spin-up and spin-down electrons, which results in the mini-gap peak splitting. For a certain value of h the mini-gap closes resulting in the DOS enhancement at zero energy as seen from Fig. 2 (b) and (c). This feature known as a zero energy peak (ZEP) has been investigated both theoretically [95-98] and experimentally [47]. Another interesting peculiarity of the DOS is the appearance of the characteristic peak at $E = h$, which arises as the exchange field exceeds the superconducting gap $h > \Delta$. Apparently, this peak arises from the evolution of the second spin split peak due to a non-zero exchange field. The existence of such an

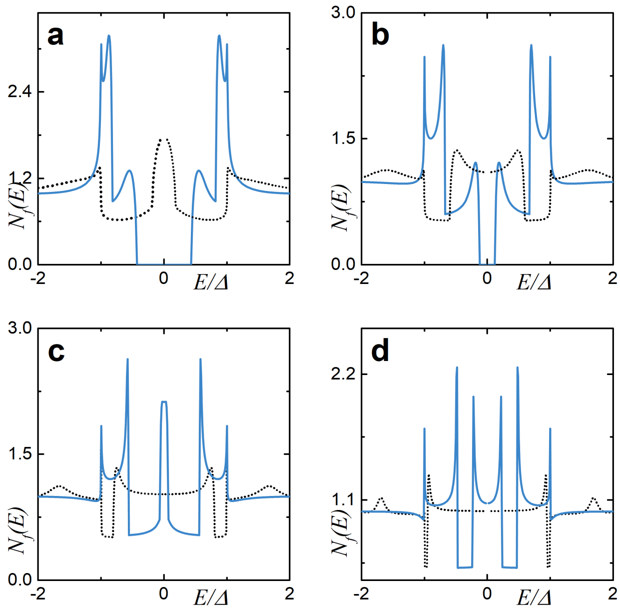

Figure 3: The evolution of the DOS plotted for increasing values of the SF interface transparencies γ_B. Here $d_f = 0.5$ and exchange field is $h = 0.4\Delta$ (blue solid line) and $h = 1.7\Delta$ (black dotted line). (a) $\gamma_B = 2$, (b) $\gamma_B = 5$, (c) $\gamma_B = 10$ and (d) $\gamma_B = 25$.

effect offers a method of determining relatively small exchange field values in F layer via the DOS measurements [46,49,99].

In Fig. 3 the DOS evolution at increasing interface parameter γ_B is shown. The blue solid line corresponds to the subgap exchange field $h = 0.4\Delta$, whereas the black dotted line to $h = 1.5\Delta$. From the figure we can notice that an increase of γ_B also has a strong influence on the DOS structure. Sufficiently large interface resistance can close the mini-gap and lead to the emergence of the ZEP (Fig. 3 (c) blue solid line). However, the peak structure is different for the two exchange fields h as seen from the figure.

In what follows, we will examine the effect produced by both spin-flip and spin-orbit scattering on the DOS features, mostly focusing on the mini-gap and the DOS peak at $E = h$. Unlike previous results on this topic [82,83], we provide both numerical and analytical results for the DOS calculation. Although the analytical expressions have rather narrow range of applicability, such limiting cases are relevant for experiments.

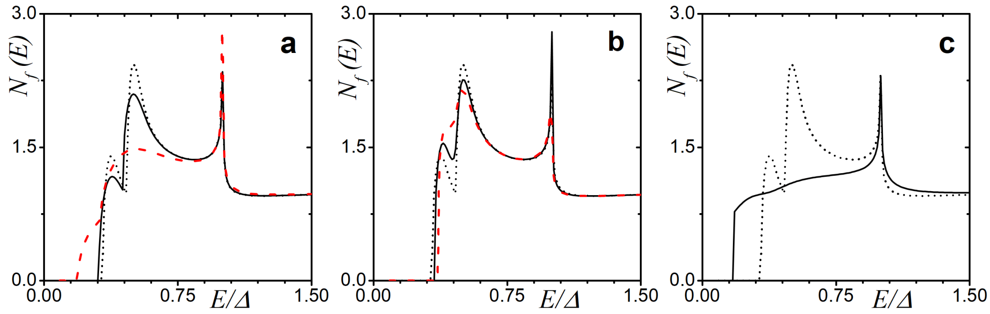

Figure 4: The DOS $N_f(E)$ on the free boundary of the F layer in the SF bilayer in the presence of magnetic and spin-orbit scattering, calculated numerically for different scattering times. The plots correspond to intermediate interface transparency $\gamma_B = 5$, $h = 0.1\Delta$, $d_f = 0.5\xi_f$. Plot (a) corresponds to $\alpha_z \neq 0$: $\alpha_z = 0.01$ (black solid line), $\alpha_z = 0.1$ (red dashed line). Plot (b) corresponds to $\alpha_{so} \neq 0$: $\alpha_{so} = 0.05$ (black solid line), $\alpha_{so} = 0.13$ (red dashed line). Plot (c) corresponds to $\alpha_x \neq 0$: $\alpha_x = 0.2$ (black solid line). Black dotted line represents $N_f(E)$ in the absence of any scattering.

Effect of scattering on the DOS features

Now we discuss the influence of the finite scattering rates on the DOS features mentioned in the previous section. In this paper we consider two cases of the junction transparency: (i) - intermediate interface transparency ($\gamma_B \geq 1$) and (ii) - low interface transparency ($\gamma_B \gg 1$). In both cases we fix the thickness of F layer to $d_f = 0.5\xi_f$. Focusing on these cases allows us to discuss all the major effects on the DOS features utilizing not only numerical solution of the problem, but also some analytical results, which will be presented below.

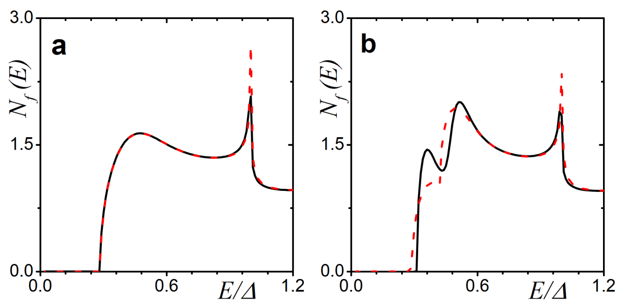

Figure 5: The DOS $N_f(E)$ on the free boundary of the F layer in the SF bilayer in the presence of magnetic scattering, calculated numerically in the case of $h = 0$ (a) and $h = 0.1\Delta$ (b), $d_f = 0.5\xi_f$. Parameters of the F/S interface are $\gamma = 0.05, \gamma_B = 5$. Plot (a) corresponds to $\alpha_x = 0.035$ (black solid line) and $\alpha_z = 0.07$ (red dashed line). Plot (b) corresponds to $\alpha_x = 0.01$ (black solid line) and $\alpha_z = 0.02$ (red dashed line).

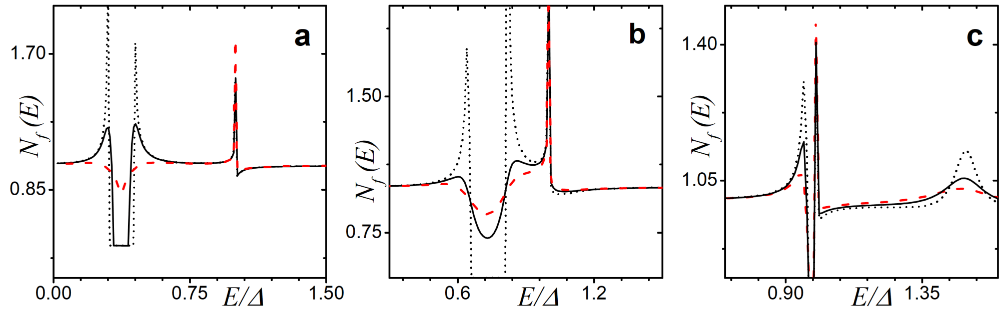

Figure 6: The DOS $N_f(E)$ on the free boundary of the F layer in the SF bilayer in the presence of magnetic scattering, calculated numerically for the low transparency interface with $\gamma_B = 50$.Plot (a) corresponds to $\alpha_z \neq 0$ and $h = 0.4\Delta$: black solid line - $\alpha_z = 0.01$, red dashed line - $\alpha_z = 0.1$. Plot (b) corresponds to $\alpha_{so} \neq 0$ and $h = 0.8\Delta$: black solid line - $\alpha_{so} = 0.05$, red dashed line- $\alpha_{so} = 0.1$. Plot (c) corresponds to $\alpha_{so} \neq 0$: black solid line - $\alpha_{so} = 0.05$, red dashed line- $\alpha_{so} = 0.1$. Black dotted line represents $N_f(E)$ in the absence of any scattering.

Intermediate interface transparency ($\gamma_B = 5$)

Fig. 4 depicts the DOS dependencies in case of relatively low interface transparency ($\gamma_B = 5$) in the presence of spin-flip and spin-orbit scattering. It is clearly seen that the decrease of the parallel magnetic scattering time leads to smearing of the split peaks with the gradual closing of the induced energy gap (mini-gap) in F layer (Fig. 4 (a)). The influence of the perpendicular magnetic scattering can be observed in Fig. 4 (c). While increasing the scattering rate α_x tends to suppress the split peaks, perpendicular magnetic scattering also moves the peaks towards Fermi energy destroying the mini-gap. One of the possible explanations is the presence of some additional field besides the ordinary exchange field in the F layer [82]. Summarizing the results of the calculations, it is obvious that the magnetic scattering tends to destroy the proximity induced superconductivity in the F layer. Such an effect becomes clear from more detailed analysis of the linearized Usadel equation (1) in the low proximity limit. In this case the anomalous Green's function is dependent on exchange field h and the magnetic scattering rates, which apparently are pair breaking as well as the exchange field.

Figure 4 (b) shows that a smaller spin-orbit scattering time leads to the vanishing of the peak splitting in the subgap region. On the contrary, though the spin-orbit scattering ruins the double peak structure due to an exchange field smearing them into one peak, it does not produce destructive effect on the mini-gap magnitude (Fig. 7 (b)). This feature has been reported previously [83].

In Fig. 5 the effect of magnetic scatterings α_z and α_x on the DOS in the SN bilayer ($h = 0$, plot a) and the SF bilayer (plot b) is demonstrated. Apparently, the uniaxial magnetic scattering has the same impact on the $N_f(E)$ as perpendicular scattering rate $\alpha_x = \alpha_z/2$ in the NS bilayer (Fig. 5 (a)). However, the situation can not take place in case of nonzero exchange field h, which we can observe from the plot (b).

Low interface transparency ($\gamma_B = 50$)

Now we focus on the limit of a highly resistive SF interface and investigate the effects of a spin-dependent scattering. As expected, the influence of the adjacent superconducting layer on the DOS is rather limited due to low transparency of the interface (Fig. 6). It can be seen that the mini-gap is hardly recognizable in the cases of both subgap values of h (Fig. 6 a, b) and $h > \Delta$ exchange field (Fig. 6 c). From the plots we can say that the finite scattering rates suppress the DOS features in the case of low interface transparency as well (Fig. 6 solid and dashed lines). Even the DOS peak at $E = h$ is suppressed substantially (Fig. 6 c). However, a closer examination shows that all the scattering rates slightly differ in a way they modify the DOS structure.

We would like to draw an attention to discuss the effect of scattering on the DOS peak located at the exchange energy in more detail. As we have mentioned above, one of the interesting features in the DOS of the considered system is the peak at $E = h$ (Fig. 7 (a)). In Fig. 7 we demonstrate the influence of different scattering rates on the DOS peak at $E = h$ using the numerically obtained results. The rest parameters used for calculations here are $\gamma_B = 50, d_f = 0.5\xi_f, h = 1.5\Delta$. In Fig. 7 (b) the plot for different values of α_z is shown. It can be noticed that the uniaxial magnetic scattering not only suppresses the peak, but also slightly shifts the DOS peak towards $E = 0$. The spin-orbit scattering has a similar effect on the peak, though α_{so} has a stronger effect on the peak height compared to α_z as it can be noticed from Fig. 7 (c) . In both cases above the DOS peak also smears as any of the scattering rates increases. The effect of the perpendicular magnetic scattering α_x is indicated in Fig. 7 (c).

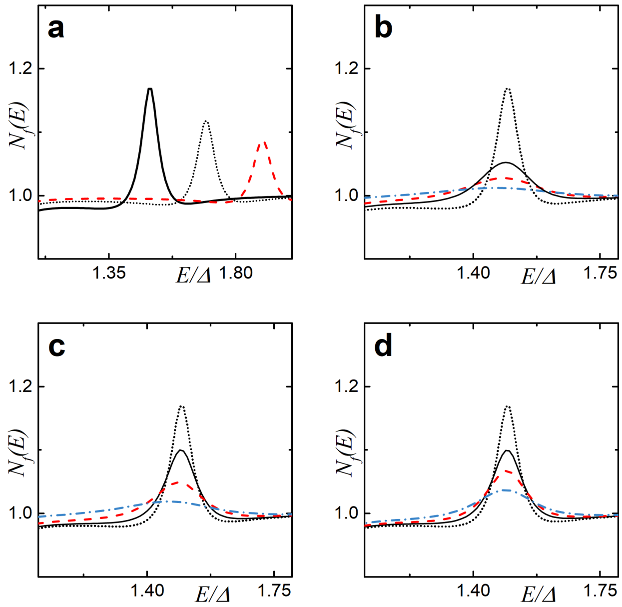

Figure 7: The peak at $E = \Delta$ in the DOS calculated numerically for three different h (a): $h = 1.4\Delta$ (black solid line), $h = 1.6\Delta$ (black dotted line) and $h = 1.9\Delta$ (red dashed line). The influence of different scatterings on the DOS peak at $E = h$ in the SF structure. Here $\gamma_B = 50, d_f = 0.5$ and exchange field is $h = 1.5\Delta$ for plots (b)-(d). In plots (b)-(d) black dotted line represents the DOS calculated in the absence of any scattering. Plot (b) corresponds to the case of nonzero α_z: black solid line - $\alpha_z = 0.05$, red dashed line - $\alpha_z = 0.1$ and blue dash-dotted line - $\alpha_z = 0.2$. Plot (c) corresponds to the case of nonzero α_{so}: black solid line - $\alpha_{so} = 0.02$, red dashed line - $\alpha_{so} = 0.06$ and blue dash-dotted line - $\alpha_{so} = 0.15$. Plot (d) corresponds to the case of nonzero α_x: black solid line - $\alpha_x = 0.02$, red dashed line - $\alpha_x = 0.04$ and blue dash-dotted line - $\alpha_x = 0.08$.

Analytical result for the interfaces with low transparency and qualitative picture

Here we employ the analytical expression (19) obtained in the low proximity and thin F layer limit. Considering the problem in such a limit makes possible to use simple expression for qualitative description of the corresponding scattering effects on the DOS structure. It should not be forgotten that the linearized solution of the form Eq. (19) is quite limited in its application. In our case it is valid when $\gamma_B \gg 1$ and $d_f \ll \min\left(\xi_f, \sqrt{D_f/h}\right)$, which is true for $\gamma_B = 50$. This tunneling limit is experimentally feasible, thus our result could easily be applied.

In Fig. 8 the DOS calculated analytically via Eq. (19) is illustrated. Here we focus on the case of zero exchange field $h = 0$ to investigate the impact of each type of scatterings on the mini-gap. We plot the analytically obtained DOS for the SN case in the absence of any scattering for comparison (black dotted line) as well. From the figure one can see that the spin-orbit scattering does not affect

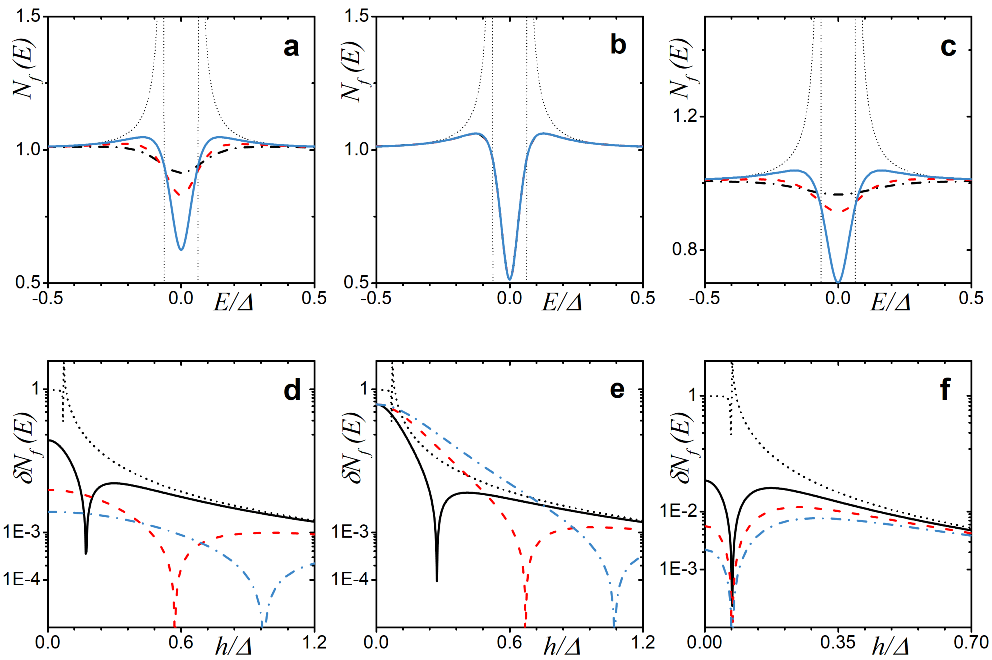

Figure 8: (Upper panel) The DOS calculated analytically in the low proximity and thin adjacent normal metal layer $h = 0$ with: (a) finite uniaxial magnetic scattering $\alpha_z > 0$ ($\alpha_x = \alpha_{so} = 0$); (b) spin-orbit scattering $\alpha_{so} > 0$ ($\alpha_z = \alpha_x = 0$); (c) magnetic scattering $\alpha_x > 0$ ($\alpha_z = \alpha_{so} = 0$). The curves calculated for $\gamma_B = 50, d_f = 0.5$. In the plots, blue solid line corresponds to $\alpha_i = 0.01$, red dashed line - $\alpha_i = 0.05$ and black dash-dotted line - $\alpha_i = 0.1$, where i - is the corresponding scattering rate. The faint black dotted line corresponds to analytical solution of Eq. (16). (Lower panel) Analytical dependence of $\delta N_f(0)$ as a function of the exchange field h for different magnetic scattering rates α_z (d), α_x (f) and spin-orbit scattering α_{so} (e). Parameters of the SF interface are $\gamma_B = 50, \gamma = 0.05$ and $d_f = 0.5\xi_f$. Black dotted line represents $\delta N_f(0)$ derived from Eq. (16). Plot (d): $\alpha_z = 0.1$ - black solid line, $\alpha_z = 0.5$ - red dashed line, $\alpha_z = 0.9$ - blue dash-dotted line. Plot (e): $\alpha_{so} = 0.1$ - black solid line, $\alpha_{so} = 0.3$ - red dashed line, $\alpha_{so} = 0.5$ - blue dash-dotted line. Plot (f): $\alpha_x = 0.3$ - black solid line, $\alpha_x = 0.5$ - red dashed line, $\alpha_x = 0.9$ - blue dash-dotted line.

the DOS in any way (Fig. 8 (b)), the effect that has been shown before numerically in Ref. [83]. On the other hand, both nonzero magnetic scatterings α_x and α_z have a strong effect on the mini-gap, leading to its complete vanishing at some value of α (Fig. 8 (a) and (c)).

Making comparisons between previous results [82,83] , we can say that there is a qualitative agreement in the DOS behavior. Indeed, in case of large DOS variations and especially singularities the analytical model introduced above may fail. Nevertheless, we can explain major features of $N_f(E)$ in the presence of a spin-dependent scattering. Examining the linearized Usadel equations we can analyze the anomalous Green's functions by studying even-frequency spin-singlet ($f_s \propto (\theta_{f\uparrow} - \theta_{f\downarrow})/2$) and odd-frequency spin-triplet ($f_t \propto (\theta_{f\uparrow} + \theta_{f\downarrow})/2$) components. When

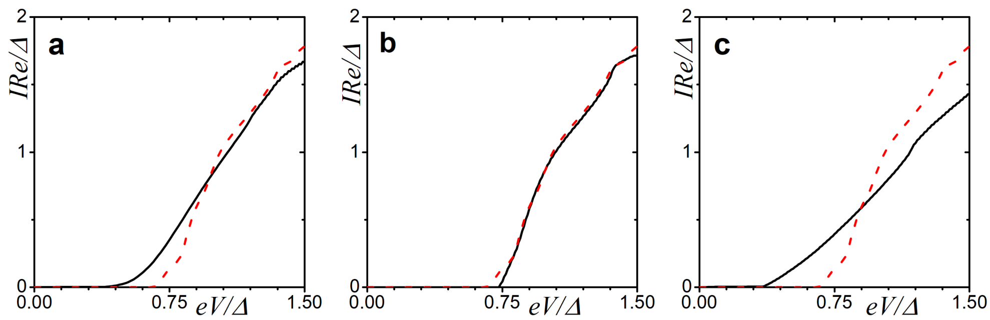

Figure 9: Current–voltage characteristics of a SFIFS junction in the presence of a spin-dependent scattering. The plots correspond to intermediate interface transparency $\gamma_B = 5$, $h = 0.1\Delta$, $d_f = 0.5\xi_f$. Plot (a) corresponds to $\alpha_z = 0.1$, plot (b) - $\alpha_{so} = 0.13$ and plot (c) - $\alpha_x = 0.2$. Red dashed line represents the case of zero scattering

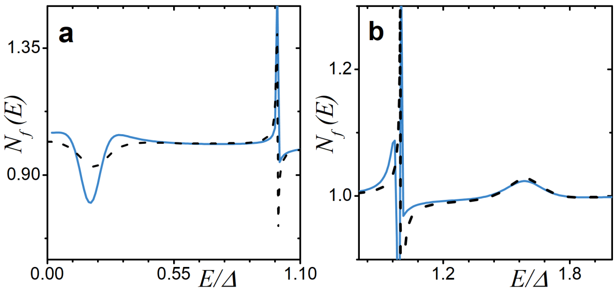

Figure 10: Comparison of the analytical result in the low proximity limit and thin adjacent ferromagnetic layer (black dashed line) with the DOS obtained numerically (blue solid line) for two different values of exchange field h. The parameters are $\gamma_B = 50, d_f = 0.5$. Plot a: $h = 0.2\Delta$, $\alpha_z = \alpha_x = \alpha_{so} = 0.02$. Plot b: $h = 1.6\Delta$, $\alpha_z = 0.02$, $\alpha_{so} = \alpha_x = 0.04$.

there is an F layer with a relatively high rate of parallel magnetic scattering we can simplify the linearized Usadel equation and obtain

$$\frac{D_f}{2}\frac{\partial^2 \theta_{f\uparrow(\downarrow)}}{\partial x^2} = \frac{1}{\tau_z}\theta_{f\uparrow(\downarrow)}. \tag{20}$$

From this equation we can find that $\theta_{f\uparrow} = \theta_{f\downarrow} = 0$ leading to supression of both the singlet and triplet components. In the presence of large in-plane magnetic scattering α_x, we get that $\theta_{f\uparrow} = \theta_{f\downarrow}$, which leads to $f_s = 0$, whereas the triplet component f_t is nonzero. This can be understood in a similar way from the linearised Usadel equation,

$$\frac{D_f}{2}\frac{\partial^2 \theta_{f\uparrow(\downarrow)}}{\partial x^2} = \frac{1}{\tau_x}(\theta_{f\uparrow} + \theta_{f\downarrow}), \tag{21}$$

Since the energy gap is defined by the singlet correlations we observe the detrimental effect of the in-plane scattering on the mini-gap magnitude (Fig. 8 (c)). On the other hand, in the limit of strong spin-orbit scattering α_{so} the Usadel equation in F layer reads,

$$\frac{D_f}{2}\frac{\partial^2\theta_{f\uparrow(\downarrow)}}{\partial x^2} = \pm\frac{1}{\tau_{so}}(\theta_{f\uparrow} - \theta_{f\downarrow}), \tag{22}$$

which results in $\theta_{f\uparrow} = -\theta_{f\downarrow}$, causing strong suppression of the triplet component and not the singlet one, which in turn explains the robustness of the mini-gap (Fig. 8 (b)). It can be demonstrated that the triplet component suppression due to spin-orbit scattering can actually lead to the appearance of the mini-gap at finite exchange fields h.

One of the possible ways of observing the the DOS features is the examination of the current-voltage characteristics. Utilizing the Werthamer expression for the quasiparticle current in tunneling junctions we can calculate the I-V curves for SFIFS junction. The current then reads,

$$I = \frac{1}{eR}\int_{-\infty}^{\infty} dE\ N_{f1}(E-eV)N_{f2}(E)[f(E-eV) - f(E)]. \tag{23}$$

Here $N_{f1,2}(E)$ is the density of states (DOS) in the corresponding ferromagnetic layer at $x = 0$, $f(E) = [1 + e^{E/T}]^{-1}$ is the Fermi-Dirac distribution function, and $R = R_{B0}$ is the resistance across the F-I-F interface. Both densities of states $N_{f1,2}(E)$ are normalized to their values in the normal state. The above mentioned effects of spin-dependent scattering have a direct influence on the current. Fig. 9 demonstrates the current-voltage characteristics of the SFIFS junction calculated in the presence of parallel magnetic (Fig. 9 (a)), spin-orbit (Fig. 9 (b)) and perpendicular magnetic scattering (Fig. 9 (c)). From the plots we can notice that while a magnetic scattering destroys the mini-gap, the spin-orbit scattering slightly enhances it.

It is interesting to plot another dependence reflecting the behavior of the DOS at zero energy. Utilizing Eq. (19), we plot $\delta N_f = |1 - N_f(E = 0)|$ as a function of the exchange field to examine the effect of finite scattering rates. In the lower panel of Fig. 8 the dependencies of δN_f on the exchange field h are presented. From the plots we may point out that the effect of uniaxial magnetic scattering (Fig. 8 (d)) acts like a combination of the spin-orbit (Fig. 8 (e)) and perpendicular magnetic (Fig. 8 (f)) scattering.

Finally, we compare the analytically derived and numerically calculated DOS in the case of the SF junction with thin F layer and low transparency interface. The corresponding result is shown in Fig. 10. We can observe fairly good agreement between the numerical and analytical calculation. As expected the analytical expression Eq. (19) can not describe the features of $N_f(E)$ which are relatively large in scale compared to unity, especially it may not give a proper quantitative description of the DOS singularities.

Conclusion

We have formulated the model, which takes into account magnetic and spin-orbit scattering processes in the framework of quasiclassical Green's function approach in the diffusive limit. Based on these equations the local density of states has been calculated numerically. Moreover, we provide relatively simple expression to calculate the DOS analytically in the presence of magnetic scattering α_z for thin F layers. In addition, the analytic solution for the anomalous Green's function has been derived in the low proximity limit and thin ferromagnetic layer. Based on this solution we have been able to present analytical result for the DOS taking into account all the spin dependent scattering. We have demonstrated that analytical result is in qualitative agreement with the numerical predictions, including previously published findings. In particular, we have found that the mini-gap is resilient upon increasing of spin-orbit scattering rate, while the magnetic scattering perpendicular to the quantization axis eventually closes the mini-gap.

Acknowledgements

Authors acknowledge support of the Mirror Laboratories joint project of the HSE University and the Bashkir State Pedagogical University.

References

1. Buzdin, A. I. *Rev. Mod. Phys.* **2005**, *77*, 935–976. doi:10.1103/RevModPhys.77.935.

2. Golubov, A. A.; Kupriyanov, M. Y.; Il'ichev, E. *Rev. Mod. Phys.* **2004**, *76*, 411–469. doi:10.1103/RevModPhys.76.411.

3. Bergeret, F. S.; Volkov, A. F.; Efetov, K. B. *Rev. Mod. Phys.* **2005**, *77*, 1321–1373. doi:10.1103/RevModPhys.77.1321.

4. Demler, E. A.; Arnold, G. B.; Beasley, M. R. *Phys. Rev. B* **1997**, *55*, 15174–15182. doi:10.1103/PhysRevB.55.15174.

5. Ozaeta, A.; Vasenko, A. S.; Hekking, F. W. J.; Bergeret, F. S. *Phys. Rev. B* **2012**, *86*, 060509. doi:10.1103/PhysRevB.86.060509.

6. Bergeret, F. S.; Tokatly, I. V. *Phys. Rev. Lett.* **2013**, *110*, 117003. doi:10.1103/PhysRevLett.110.117003.

7. Khaydukov, Y.; Pütter, S.; Guasco, L.; Morari, R.; Kim, G.; Keller, T.; Sidorenko, A.; Keimer, B. *Beilstein Journal of Nanotechnology* **2020**, *11*, 1254–1263. doi:10.3762/bjnano.11.109.

8. Klenov, N.; Khaydukov, Y.; Bakurskiy, S.; Morari, R.; Soloviev, I.; Boian, V.; Keller, T.; Kupriyanov, M.; Sidorenko, A.; Keimer, B. *Beilstein Journal of Nanotechnology* **2020**, *10*, 833–839. doi:10.3762/bjnano.10.83.

9. Bakurskiy, S.; Kupriyanov, M.; Klenov, N. V.; Soloviev, I.; Schegolev, A.; Morari, R.; Khaydukov, Y.; Sidorenko, A. S. *Beilstein Journal of Nanotechnology* **2020**, *11*, 1336–1345. doi:10.3762/bjnano.11.118.

10. Marychev, D. Y., P. M. Vodolazov *Beilstein Journal of Nanotechnology* **2020**, *11*, 858—865. doi:10.3762/bjnano.11.71.

11. Jiang, J. S.; Davidović, D.; Reich, D. H.; Chien, C. L. *Phys. Rev. Lett.* **1995**, *74*, 314–317. doi:10.1103/PhysRevLett.74.314.

12. Izyumov, Y. A.; Proshin, Y. N.; Khusainov, M. G. *Phys. Usp.* **2002**, *45* (2), 109–148. doi:10.1070/PU2002v045n02ABEH001025.

13. Fominov, Y. V.; Chtchelkatchev, N. M.; Golubov, A. A. *Phys. Rev. B* **2002**, *66*, 014507. doi:10.1103/PhysRevB.66.014507.

14. Khaydukov, Y. N.; Vasenko, A. S.; Kravtsov, E. A.; Progliado, V. V.; Zhaketov, V. D.; Csik, A.; Nikitenko, Y. V.; Petrenko, A. V.; Keller, T.; Golubov, A. A.; Kupriyanov, M. Y.; Ustinov, V. V.; Aksenov, V. L.; Keimer, B. *Phys. Rev. B* **2018**, *97*, 144511. doi:10.1103/PhysRevB.97.144511.

15. Karabassov, T.; Stolyarov, V. S.; Golubov, A. A.; Silkin, V. M.; Bayazitov, V. M.; Lvov, B. G.; Vasenko, A. S. *Phys. Rev. B* **2019**, *100*, 104502. doi:10.1103/PhysRevB.100.104502.

16. Karabassov, T.; Golubov, A. A.; Silkin, V. M.; Stolyarov, V. S.; Vasenko, A. S. *Phys. Rev. B* **2021**, *103*, 224508. doi:10.1103/PhysRevB.103.224508.

17. Buzdin, A. I.; Bulaevskii, L. N.; Panyukov, S. V. *JETP Letters* **1982**, *35* (5), 178.

18. Vdovichev, S. N.; Nozdrin, Y. N.; Pestov, E. E.; Yunin, P. A.; Samokhvalov, A. V. *JETP Letters* **2016**, *104* (5), 329–333. doi:10.1134/S0021364016170148.

19. Ryazanov, V. V.; Oboznov, V. A.; Rusanov, A. Y.; Veretennikov, A. V.; Golubov, A. A.; Aarts, J. *Phys. Rev. Lett.* **2001**, *86*, 2427–2430. doi:10.1103/PhysRevLett.86.2427.

20. Ryazanov, V. V.; Oboznov, V. A.; Veretennikov, A. V.; Rusanov, A. Y. *Phys. Rev. B* **2001**, *65*, 020501. doi:10.1103/PhysRevB.65.020501.

21. Blum, Y.; Tsukernik, A.; Karpovski, M.; Palevski, A. *Phys. Rev. Lett.* **2002**, *89*, 187004. doi:10.1103/PhysRevLett.89.187004.

22. Sellier, H.; Baraduc, C.; Lefloch, F. m. c.; Calemczuk, R. *Phys. Rev. Lett.* **2004**, *92*, 257005. doi:10.1103/PhysRevLett.92.257005.

23. Bauer, A.; Bentner, J.; Aprili, M.; Della Rocca, M. L.; Reinwald, M.; Wegscheider, W.; Strunk, C. *Phys. Rev. Lett.* **2004**, *92*, 217001. doi:10.1103/PhysRevLett.92.217001.

24. Bell, C.; Loloee, R.; Burnell, G.; Blamire, M. G. *Phys. Rev. B* **2005**, *71*, 180501. doi:10.1103/PhysRevB.71.180501.

25. Oboznov, V. A.; Bol'ginov, V. V.; Feofanov, A. K.; Ryazanov, V. V.; Buzdin, A. I. *Phys. Rev. Lett.* **2006**, *96*, 197003. doi:10.1103/PhysRevLett.96.197003.

26. Shelukhin, V.; Tsukernik, A.; Karpovski, M.; Blum, Y.; Efetov, K. B.; Volkov, A. F.; Champel, T.; Eschrig, M.; Löfwander, T.; Schön, G.; Palevski, A. *Phys. Rev. B* **2006**, *73*, 174506. doi:10.1103/PhysRevB.73.174506.

27. Vasenko, A. S.; Golubov, A. A.; Kupriyanov, M. Y.; Weides, M. *Phys. Rev. B* **2008**, *77*, 134507. doi:10.1103/PhysRevB.77.134507.

28. Anwar, M. S.; Czeschka, F.; Hesselberth, M.; Porcu, M.; Aarts, J. *Phys. Rev. B* **2010**, *82*, 100501. doi:10.1103/PhysRevB.82.100501.

29. Khaire, T. S.; Khasawneh, M. A.; Pratt, W. P.; Birge, N. O. *Phys. Rev. Lett.* **2010**, *104*, 137002. doi:10.1103/PhysRevLett.104.137002.

30. Robinson, J. W. A.; Witt, J. D. S.; Blamire, M. G. *Science* **2010**, *329* (5987), 59–61. doi:10.1126/science.1189246.

31. Baker, T. E.; Richie-Halford, A.; Icreverzi, O. E.; Bill, A. *EPL (Europhysics Letters)* **2014**, *107* (1), 17001. doi:10.1209/0295-5075/107/17001.

32. Alidoust, M.; Halterman, K. *Phys. Rev. B* **2014**, *89*, 195111. doi:10.1103/PhysRevB.89.195111.

33. Loria, R.; Meneghini, C.; Torokhtii, K.; Tortora, L.; Pompeo, N.; Cirillo, C.; Attanasio, C.; Silva, E. *Phys. Rev. B* **2015**, *92*, 184106. doi:10.1103/PhysRevB.92.184106.

34. Bakurskiy, S. V.; Filippov, V. I.; Ruzhickiy, V. I.; Klenov, N. V.; Soloviev, I. I.; Kupriyanov, M. Y.; Golubov, A. A. *Phys. Rev. B* **2017**, *95*, 094522. doi:10.1103/PhysRevB.95.094522.

35. Yamashita, T.; Kawakami, A.; Terai, H. *Phys. Rev. Applied* **2017**, *8*, 054028. doi:10.1103/PhysRevApplied.8.054028.

36. Kontos, T.; Aprili, M.; Lesueur, J.; Genêt, F.; Stephanidis, B.; Boursier, R. *Phys. Rev. Lett.* **2002**, *89*, 137007. doi:10.1103/PhysRevLett.89.137007.

37. Guichard, W.; Aprili, M.; Bourgeois, O.; Kontos, T.; Lesueur, J.; Gandit, P. *Phys. Rev. Lett.* **2003**, *90*, 167001. doi:10.1103/PhysRevLett.90.167001.

38. Born, F.; Siegel, M.; Hollmann, E. K.; Braak, H.; Golubov, A. A.; Gusakova, D. Y.; Kupriyanov, M. Y. *Phys. Rev. B* **2006**, *74*, 140501. doi:10.1103/PhysRevB.74.140501.

39. Pepe, G. P.; Latempa, R.; Parlato, L.; Ruotolo, A.; Ausanio, G.; Peluso, G.; Barone, A.; Golubov, A. A.; Fominov, Y. V.; Kupriyanov, M. Y. *Phys. Rev. B* **2006**, *73*, 054506. doi:10.1103/PhysRevB.73.054506.

40. Weides, M.; Kemmler, M.; Goldobin, E.; Koelle, D.; Kleiner, R.; Kohlstedt, H.; Buzdin, A. *Applied Physics Letters* **2006**, *89* (12), 122511. doi:10.1063/1.2356104.

41. Weides, M.; Kemmler, M.; Kohlstedt, H.; Waser, R.; Koelle, D.; Kleiner, R.; Goldobin, E. *Phys. Rev. Lett.* **2006**, *97*, 247001. doi:10.1103/PhysRevLett.97.247001.

42. Weides, M.; Schindler, C.; Kohlstedt, H. *Journal of Applied Physics* **2007**, *101* (6), 063902. doi:10.1063/1.2655487.

43. Bannykh, A. A.; Pfeiffer, J.; Stolyarov, V. S.; Batov, I. E.; Ryazanov, V. V.; Weides, M. *Phys. Rev. B* **2009**, *79*, 054501. doi:10.1103/PhysRevB.79.054501.

44. Kemmler, M.; Weides, M.; Weiler, M.; Opel, M.; Goennenwein, S. T. B.; Vasenko, A. S.; Golubov, A. A.; Kohlstedt, H.; Koelle, D.; Kleiner, R.; Goldobin, E. *Phys. Rev. B* **2010**, *81*, 054522. doi:10.1103/PhysRevB.81.054522.

45. Pfeiffer, J.; Kemmler, M.; Koelle, D.; Kleiner, R.; Goldobin, E.; Weides, M.; Feofanov, A. K.; Lisenfeld, J.; Ustinov, A. V. *Phys. Rev. B* **2008**, *77*, 214506. doi:10.1103/PhysRevB.77.214506.

46. Buzdin, A. *Phys. Rev. B* **2000**, *62*, 11377–11379. doi:10.1103/PhysRevB.62.11377.

47. Kontos, T.; Aprili, M.; Lesueur, J.; Grison, X. *Phys. Rev. Lett.* **2001**, *86*, 304–307. doi:10.1103/PhysRevLett.86.304.

48. Halterman, K.; Valls, O. T. *Phys. Rev. B* **2004**, *69*, 014517. doi:10.1103/PhysRevB.69.014517.

49. Vasenko, A. S.; Kawabata, S.; Golubov, A. A.; Kupriyanov, M. Y.; Lacroix, C.; Bergeret, F. S.; Hekking, F. W. J. *Phys. Rev. B* **2011**, *84*, 024524. doi:10.1103/PhysRevB.84.024524.

50. Kontos, T.; Aprili, M.; Lesueur, J.; Grison, X.; Dumoulin, L. *Phys. Rev. Lett.* **2004**, *93*, 137001. doi:10.1103/PhysRevLett.93.137001.

51. Buzdin, A. *Phys. Rev. Lett.* **2008**, *101*, 107005. doi:10.1103/PhysRevLett.101.107005.

52. Pugach, N. G.; Goldobin, E.; Kleiner, R.; Koelle, D. *Phys. Rev. B* **2010**, *81*, 104513. doi:10.1103/PhysRevB.81.104513.

53. Pugach, N. G.; Kupriyanov, M. Y.; Vedyayev, A. V.; Lacroix, C.; Goldobin, E.; Koelle, D.; Kleiner, R.; Sidorenko, A. S. *Phys. Rev. B* **2009**, *80*, 134516. doi:10.1103/PhysRevB.80.134516.

54. Volkov, A. F.; Efetov, K. B. *Phys. Rev. Lett.* **2009**, *103*, 037003. doi:10.1103/PhysRevLett.103.037003.

55. Mai, S.; Kandelaki, E.; Volkov, A. F.; Efetov, K. B. *Phys. Rev. B* **2011**, *84*, 144519. doi:10.1103/PhysRevB.84.144519.

56. Karabassov, T.; Guravova, A. V.; Kuzin, A. Y.; Kazakova, E. A.; Kawabata, S.; Lvov, B. G.; Vasenko, A. S. *Beilstein Journal of Nanotechnology* **2020**, *11*, 252–262. doi:10.3762/bjnano.11.19.

57. Bobkova, I. V.; Bobkov, A. M. *Phys. Rev. B* **2017**, *96*, 104515. doi:10.1103/PhysRevB.96.104515.

58. Linder, J.; Bathen, M. E. *Phys. Rev. B* **2016**, *93*, 224509. doi:10.1103/PhysRevB.93.224509.

59. Machon, P.; Eschrig, M.; Belzig, W. *Phys. Rev. Lett.* **2013**, *110*, 047002. doi:10.1103/PhysRevLett.110.047002.

60. Ozaeta, A.; Virtanen, P.; Bergeret, F. S.; Heikkilä, T. T. *Phys. Rev. Lett.* **2014**, *112*, 057001. doi:10.1103/PhysRevLett.112.057001.

61. Kolenda, S.; Wolf, M. J.; Beckmann, D. *Phys. Rev. Lett.* **2016**, *116*, 097001. doi:10.1103/PhysRevLett.116.097001.

62. Giazotto, F.; Robinson, J. W. A.; Moodera, J. S.; Bergeret, F. S. *Applied Physics Letters* **2014**, *105* (6), 062602. doi:10.1063/1.4893443.

63. Giazotto, F.; Heikkilä, T. T.; Bergeret, F. S. *Phys. Rev. Lett.* **2015**, *114*, 067001. doi:10.1103/PhysRevLett.114.067001.

64. Bobkova, I. V.; Bobkov, A. M.; Belzig, W. *Phys. Rev. B* **2021**, *103*, L020503. doi:10.1103/PhysRevB.103.L020503.

65. Tagirov, L. R. *Phys. Rev. Lett.* **1999**, *83*, 2058–2061. doi:10.1103/PhysRevLett.83.2058.

66. Huertas-Hernando, D.; Nazarov, Y. V.; Belzig, W. *Phys. Rev. Lett.* **2002**, *88*, 047003. doi:10.1103/PhysRevLett.88.047003.

67. Giazotto, F.; Taddei, F. *Phys. Rev. B* **2008**, *77*, 132501. doi:10.1103/PhysRevB.77.132501.

68. Giazotto, F.; Bergeret, F. S. *Applied Physics Letters* **2013**, *102* (16), 162406. doi:10.1063/1.4802953.

69. Alidoust, M.; Halterman, K.; Valls, O. T. *Phys. Rev. B* **2015**, *92*, 014508. doi:10.1103/PhysRevB.92.014508.

70. Halterman, K.; Alidoust, M. *Phys. Rev. B* **2016**, *94*, 064503. doi:10.1103/PhysRevB.94.064503.

71. Halterman, K.; Alidoust, M. *Superconductor Science and Technology* **2016**, *29* (5), 055007. doi:10.1088/0953-2048/29/5/055007.

72. Srivastava, A.; Olde Olthof, L. A. B.; Di Bernardo, A.; Komori, S.; Amado, M.; Palomares-Garcia, C.; Alidoust, M.; Halterman, K.; Blamire, M. G.; Robinson, J. W. A. *Phys. Rev. Applied* **2017**, *8*, 044008. doi:10.1103/PhysRevApplied.8.044008.

73. Halterman, K.; Alidoust, M. *Phys. Rev. B* **2018**, *98*, 134510. doi:10.1103/PhysRevB.98.134510.

74. Ozaeta, A.; Vasenko, A. S.; Hekking, F. W. J.; Bergeret, F. S. *Phys. Rev. B* **2012**, *85*, 174518. doi:10.1103/PhysRevB.85.174518.

75. Kawabata, S.; Ozaeta, A.; Vasenko, A. S.; Hekking, F. W. J.; Sebastián Bergeret, F. *Applied Physics Letters* **2013**, *103* (3), 032602. doi:10.1063/1.4813599.

76. Gordeeva, A. V.; Pankratov, A. L.; Pugach, N. G.; Vasenko, A. S.; Zbrozhek, V. O.; Blagodatkin, A. V.; Pimanov, D. A.; Kuzmin, L. S. *Scientific Reports* **2020**, *10*, 21961. doi:10.1038/s41598-020-78869-z.

77. Golubov, A. A.; Kupriyanov, M. Y. *Journal of Low Temperature Physics* **1988**, *70* (1), 83–130. doi:10.1007/BF00683247.

78. Crouzy, B.; Bascones, E.; Ivanov, D. A. *Phys. Rev. B* **2005**, *72*, 092501. doi:10.1103/PhysRevB.72.092501.

79. Golubov, A.; Kupriyanov, M.; Lesueur, J.; Siegel, M. *JETP Letters* **2005**, *81*, 217–221. doi:10.1134/1.1914877.

80. Houzet, M.; Vinokur, V.; Pistolesi, F. *Phys. Rev. B* **2005**, *72*, 220506. doi:10.1103/PhysRevB.72.220506.

81. Kuprianov, M. Y.; Lukichev, V. F. *Journal of Experimental and Theoretical Physics Letters* **1988**, *67*, 1163.

82. Gusakova, D. Y.; Golubov, A. A.; Kupriyanov, M. Y.; Buzdin, A. *Journal of Experimental and Theoretical Physics Letters* **2006**, *83* (8), 327–331. doi:10.1134/S0021364006080066.

83. Linder, J.; Yokoyama, T.; Sudbø, A. *Phys. Rev. B* **2008**, *77*, 174514. doi:10.1103/PhysRevB.77.174514.

84. Yoshizaki, D.; Golubov, A. A.; Tanaka, Y.; Asano, Y. *Japanese Journal of Applied Physics* **2011**, *51* (1), 010108. doi:10.1143/jjap.51.010108.

85. Cottet, A.; Linder, J. *Phys. Rev. B* **2009**, *79*, 054518. doi:10.1103/PhysRevB.79.054518.

86. Bezuglyi, E. V.; Vasenko, A. S.; Shumeiko, V. S.; Wendin, G. *Phys. Rev. B* **2005**, *72*, 014501. doi:10.1103/PhysRevB.72.014501.

87. Bezuglyi, E. V.; Vasenko, A. S.; Bratus, E. N.; Shumeiko, V. S.; Wendin, G. *Phys. Rev. B* **2006**, *73*, 220506. doi:10.1103/PhysRevB.73.220506.

88. Vasenko, A. S.; Hekking, F. W. J. *Journal of Low Temperature Physics* **2009**, *154* (5), 221–232. doi:10.1007/s10909-009-9869-z.

89. Arutyunov, K. Y.; Auraneva, H.-P.; Vasenko, A. S. *Phys. Rev. B* **2011**, *83*, 104509. doi:10.1103/PhysRevB.83.104509.

90. Arutyunov, K. Y.; Chernyaev, S. A.; Karabassov, T.; Lvov, D. S.; Stolyarov, V. S.; Vasenko, A. S. *Journal of Physics: Condensed Matter* **2018**, *30* (34), 343001. doi:10.1088/1361-648x/aad3ea.

91. Usadel, K. D. *Phys. Rev. Lett.* **1970**, *25*, 507–509. doi:10.1103/PhysRevLett.25.507.

92. Belzig, W.; Wilhelm, F. K.; Bruder, C.; Schön, G.; Zaikin, A. D. *Superlattices and Microstructures* **1999**, *25* (5), 1251 –1288. doi:10.1006/spmi.1999.0710.

93. Fauré, M.; Buzdin, A. I.; Golubov, A. A.; Kupriyanov, M. Y. *Phys. Rev. B* **2006**, *73*, 064505. doi:10.1103/PhysRevB.73.064505.

94. McMillan, W. L. *Phys. Rev.* **1968**, *175*, 537–542. doi:10.1103/PhysRev.175.537.

95. Zareyan, M.; Belzig, W.; Nazarov, Y. V. *Phys. Rev. Lett.* **2001**, *86*, 308–311. doi:10.1103/PhysRevLett.86.308.

96. Yokoyama, T.; Tanaka, Y.; Golubov, A. A. *Phys. Rev. B* **2005**, *72*, 052512. doi:10.1103/PhysRevB.72.052512.

97. Yokoyama, T.; Tanaka, Y.; Golubov, A. A. *Phys. Rev. B* **2006**, *73*, 094501. doi:10.1103/PhysRevB.73.094501.

98. Yokoyama, T.; Tanaka, Y.; Golubov, A. A. *Phys. Rev. B* **2007**, *75*, 134510. doi:10.1103/PhysRevB.75.134510.

99. Vasenko, A.; Kawabata, S.; Ozaeta, A.; Golubov, A.; Stolyarov, V.; Bergeret, F.; Hekking, F. *Journal of Magnetism and Magnetic Materials* **2015**, *383*, 175 –179. doi:10.1016/j.jmmm.2014.11.009.